Age of Jupiter inferred from the distinct genetics and formation times of meteorites

Thomas S. Kruijer[a,b,1], Christoph Burkhardt[a], Gerrit Budde[a], and Thorsten Kleine[a]

[a]Institut für Planetologie, University of Münster, 48149 Muenster, Germany; and [b]Nuclear and Chemical Sciences Division, Lawrence Livermore National Laboratory, Livermore, CA 94550

Edited by Neta A. Bahcall, Princeton University, Princeton, NJ, and approved May 4, 2017 (received for review March 23, 2017)

The age of Jupiter, the largest planet in our Solar System, is still unknown. Gas-giant planet formation likely involved the growth of large solid cores, followed by the accumulation of gas onto these cores. Thus, the gas-giant cores must have formed before dissipation of the solar nebula, which likely occurred within less than 10 My after Solar System formation. Although such rapid accretion of the gas-giant cores has successfully been modeled, until now it has not been possible to date their formation. Here, using molybdenum and tungsten isotope measurements on iron meteorites, we demonstrate that meteorites derive from two genetically distinct nebular reservoirs that coexisted and remained spatially separated between ∼1 My and ∼3–4 My after Solar System formation. The most plausible mechanism for this efficient separation is the formation of Jupiter, opening a gap in the disk and preventing the exchange of material between the two reservoirs. As such, our results indicate that Jupiter's core grew to ∼20 Earth masses within <1 My, followed by a more protracted growth to ∼50 Earth masses until at least ∼3–4 My after Solar System formation. Thus, Jupiter is the oldest planet of the Solar System, and its solid core formed well before the solar nebula gas dissipated, consistent with the core accretion model for giant planet formation.

Jupiter | giant planet formation | nucleosynthetic isotope anomalies | Hf-W chronometry | solar nebula

The formation of gas-giant planets such as Jupiter and Saturn is thought to have involved the growth of large solid cores of ∼10–20 Earth masses (M_E), followed by the accumulation of gas onto these cores (1, 2). Thus, the gas-giant cores must have formed before dissipation of the solar nebula—the gaseous circumstellar disk surrounding the young Sun—which likely occurred between 1 My and 10 My after Solar System formation (3). Although such rapid accretion of the gas-giant cores has successfully been modeled (1, 2, 4), until now it has not been possible to actually date their formation. Here we show that the growth of Jupiter can be dated using the distinct genetic heritage and formation times of meteorites.

Most meteorites derive from small bodies located in the main asteroid belt between Mars and Jupiter. Originally these bodies probably formed at a much wider range of heliocentric distances, as suggested by the distinct chemical and isotopic compositions of meteorites (5–8) and by dynamical models indicating that the gravitational influence of the gas giants led to scattering of small bodies into the asteroid belt (9, 10). Information on the initial formation location of meteorite parent bodies within the solar accretion disk can be obtained from nucleosynthetic isotope anomalies in meteorites. These anomalies arise through the heterogeneous distribution of isotopically anomalous presolar components and vary as a function of heliocentric distance (6, 11). For instance, Cr, Ti, and Mo isotope anomalies (6–8, 12) reveal a fundamental dichotomy in the genetic heritage of meteorites, distinguishing between "noncarbonaceous" and "carbonaceous" meteorite reservoirs (11). This distinction may reflect either a temporal change in disk composition or the separation of materials accreted inside [noncarbonaceous (NC) meteorites] and outside [carbonaceous (CC) meteorites] the orbit of Jupiter (11–14). If the latter is correct, then the age of Jupiter can be determined by assessing the formation time and longevity of the NC and CC meteorite reservoirs. However, it is currently not known when these two reservoirs formed and whether and for how long they remained isolated from each other.

To address these issues and to ultimately determine the timescale of Jupiter's formation, we obtained W and Mo isotopic data for iron meteorites (*Materials and Methods*, *SI Materials and Methods*, Fig. S1, and Tables S1–S4). These samples are fragments of the metallic cores from some of the earliest-formed planetesimals (15), making them ideal samples to search for the effects of giant planet formation on the dynamics of the early Solar System. Previous W isotope studies on iron meteorites have focused on the major groups (i.e., IIAB, IID, IIIAB, IVA, and IVB) and on determining the timescales and processes of core formation in these bodies (15). Here we extend these studies by examining a larger set of iron meteorite groups (i.e., IC, IIC, IID, IIF, IIIE, and IIIF), for which we determined the timing of core formation using the ^{182}Hf–^{182}W chronometer (half-life = 8.9 My), as well as nucleosynthetic Mo isotopic signatures, which enables us to link these irons to either the NC or the CC meteorites.

CC and NC Iron Meteorites

The Mo isotopic data reveal variable nucleosynthetic anomalies in iron meteorites (Fig. 1). Consistent with prior studies (6), we find that these anomalies predominantly reflect the heterogeneous distribution of a presolar carrier enriched in Mo nuclides produced in the slow neutron capture process (*s*-process) of nucleosynthesis (Fig. 1). However, in a plot of ε^{95}Mo vs. ε^{94}Mo (the parts per 10,000 deviations of ^{95}Mo/^{96}Mo and ^{94}Mo/^{96}Mo from terrestrial standard values), the iron meteorites fall onto

Significance

Jupiter is the most massive planet of the Solar System and its presence had an immense effect on the dynamics of the solar accretion disk. Knowing the age of Jupiter, therefore, is key for understanding how the Solar System evolved toward its present-day architecture. However, although models predict that Jupiter formed relatively early, until now, its formation has never been dated. Here we show through isotope analyses of meteorites that Jupiter's solid core formed within only ∼1 My after the start of Solar System history, making it the oldest planet. Through its rapid formation, Jupiter acted as an effective barrier against inward transport of material across the disk, potentially explaining why our Solar System lacks any super-Earths.

Author contributions: T.S.K. and T.K. designed research; T.S.K. and C.B. performed research; T.S.K., C.B., G.B., and T.K. analyzed data; and T.S.K., C.B., G.B., and T.K. wrote the paper.

The authors declare no conflict of interest.

This article is a PNAS Direct Submission.

[1]To whom correspondence should be addressed. Email: thomaskruijer@gmail.com.

This article contains supporting information online at www.pnas.org/lookup/suppl/doi:10.1073/pnas.1704461114/-/DCSupplemental.

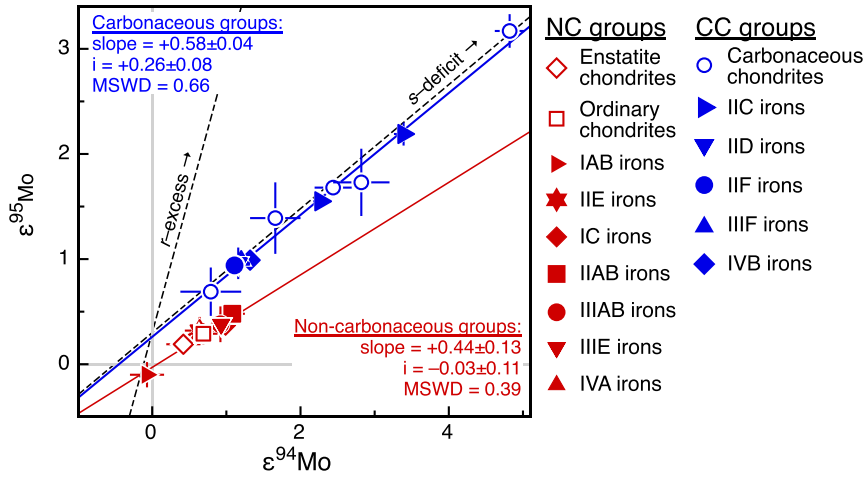

Fig. 1. Molybdenum isotope dichotomy of iron meteorite groups. Iron meteorites and chondrites define two distinct trends in ε^{95}Mo vs. ε^{94}Mo space, separating a CC (blue symbols) from a NC reservoir (red symbols). Note that the two regressions (solid lines) through the iron meteorite and chondrites from NC and CC reservoirs yield significantly different ε^{95}Mo intercept values. Error bars denote 95% conf. limits on group mean values. Also shown are *s*-process and *r*-process mixing lines (dashed lines), plotted at an ordinate ε^{95}Mo of +0.3 and calculated using the Mo isotopic composition of presolar SiC grains (37), representing *s*-process Mo and the corresponding *r*-process residuals. Note that other Mo isotopes show consistent systematics (Fig. S5). Data for IC, IIC, IID, IIF, IIIF, and IIIE iron meteorites are from this study and data for chondrites and other iron meteorite groups are from ref. 6.

two distinct *s*-process mixing lines. Whereas most of the newly investigated irons (IIC, IID, IIF, and IIIF) plot on an *s*-process mixing line together with carbonaceous chondrites, most of the previously studied irons as well as the IC and IIIE irons plot on another *s*-process mixing line together with ordinary chondrites, enstatite chondrites, and the Earth's mantle (ε^{i}Mo = 0) (Fig. 1). Thus, several iron meteorite groups (IIC, IID, IIF, IIIF, and IVB) belong to the CC meteorites, whereas several other groups (IC, IIAB, IIIAB, IIIE, and IVA) belong to the NC meteorites (Fig. 1).

A similar genetic dichotomy is seen for W isotopes, which for iron meteorites reveal two distinct clusters of ε^{182}W and ε^{183}W (the parts per 10,000 deviations of ^{182}W/^{184}W and ^{183}W/^{184}W from terrestrial standard values). The NC irons have ε^{182}W values between approximately –3.4 and –3.3 and no nucleosynthetic W isotope anomalies (i.e., ε^{183}W ~ 0), whereas the CC irons have ε^{182}W values of around –3.2 and show nucleosynthetic ε^{183}W excesses (Fig. 2, Fig. S2, and Table S5). Note that the ε^{182}W values of each group were corrected for the effects of cosmic ray exposure (Figs. S3 and S4 and Table S5), using Pt isotopes as the neutron dosimeter (15). In addition, for the iron groups showing ^{183}W anomalies, the ε^{182}W values were corrected for nucleosynthetic ε^{182}W variations, by using correlated ε^{182}W–ε^{183}W variations induced by nucleosynthetic isotope heterogeneities (15) (see *SI Text* for details).

As variable ε^{182}W values in iron meteorites reflect different times of Hf/W fractionation during metal–silicate separation on their parent bodies (15–17), the higher ε^{182}W of the CC irons indicates a later time of core formation (Table S5), at ~2.2 My to ~2.8 My, compared with the NC irons, at ~0.3 My to ~1.8 My after the start of Solar System history [as defined by the formation of Ca-Al–rich inclusions (CAI)]. A prior study has shown that ε^{182}W differences between different groups of iron meteorites could be due to distinct melting temperatures during core formation, reflecting the different S contents and hence liquidus temperatures of the cores (15). However, the NC and CC reservoirs both include iron meteorite groups with similar volatile element concentrations and, hence, presumably similar S contents. Thus, different melting temperatures of the NC and CC parent bodies cannot be the cause of the observed ε^{182}W dichotomy. Instead, the difference in core formation times is most easily explained by different accretion times of the CC and NC iron meteorite parent bodies. Thermal modeling of bodies internally heated by ^{26}Al decay (*SI Text*) shows that the NC iron meteorite parent bodies probably accreted within <0.4 My after CAI formation, whereas the CC iron meteorite parent bodies accreted slightly later, at $0.9^{+0.4}_{-0.2}$ My after CAI formation (Fig. 3). Taken together, the Mo and W isotopic data thus indicate that accretion of CC and NC iron meteorite parent bodies occurred not only in genetically distinct nebular regions, but also at different times (Figs. 2 and 3).

Coexistence and Spatial Separation of CC and NC Meteorite Reservoirs

The distinct genetic heritage and accretion times of iron meteorite parent bodies make it possible to constrain the formation time and longevity of the NC and CC nebular reservoirs. Accretion of CC iron meteorite parent bodies at ~1 My after CAI formation

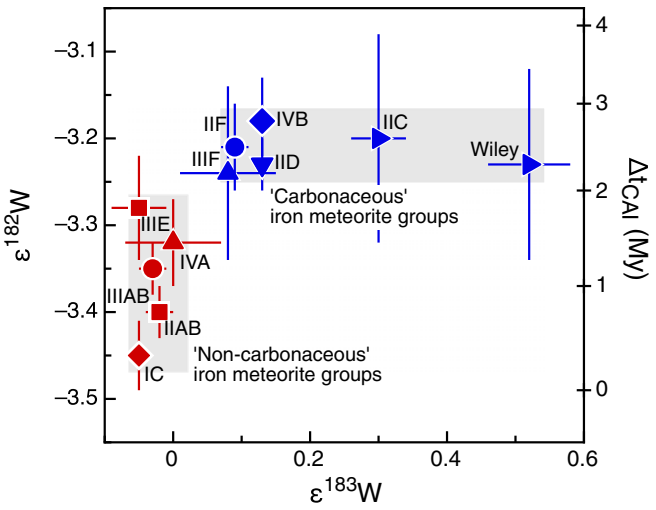

Fig. 2. Tungsten isotope dichotomy of iron meteorite groups. Error bars denote 95% conf. intervals on group mean values. ε^{182}W signatures were corrected for effects of nucleosynthetic heterogeneity and secondary neutron capture (*SI Text*). Plotted on the right ordinate axis are two-stage Hf-W model ages of core formation (see *SI Text* for details). See Fig. 1 for symbol legend.

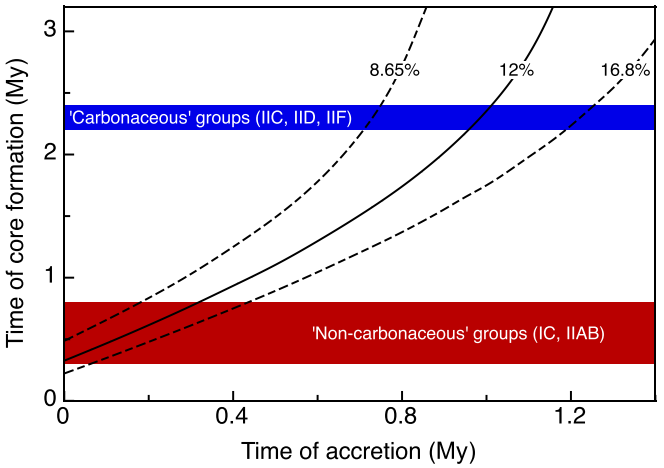

Fig. 3. Relation between the time of accretion and core formation on iron meteorite parent bodies. Curves show thermal modeling results quantifying the relation between the time of core formation and the time of parent body accretion (*SI Text*), for different Al concentrations of the bulk parent bodies (for 8.65 wt%, 12 wt%, and 16.8 wt% Al). Colored areas show the observed core formation ages of NC iron meteorite parent bodies and CC parent bodies.

implies that by this time, the NC and CC reservoirs were already separated. The distinction between the NC and CC reservoirs most likely reflects the addition of presolar material enriched in *r*-process nuclides to the solar nebula region from which the CC meteorites derive (12). Given that all CC meteorites plot on a single *s*-process mixing line with a constant offset compared with the NC line (Fig. 1), they all have the same *r*-process excess relative to the NC meteorites. Consequently, this *r*-process component must have been added to and homogeneously distributed within the CC reservoir before the first CC bodies formed. The ^{182}W data for the CC irons, therefore, indicate that this addition of material and, hence, the formation of the CC reservoir occurred within ∼1 My of Solar System formation.

A key constraint from our results is that the accretion of ordinary chondrite parent bodies in the NC reservoir (i.e., at ∼2 My) (18) occurred after the accretion of iron meteorite parent bodies in the CC reservoir (at ∼1 My). Thus, the existence of the NC and CC reservoirs cannot simply reflect a compositional change of the solar nebula over time. Instead, the CC and NC nebular reservoirs must have existed contemporaneously and remained spatially separated within the solar circumstellar disk. The timespan over which this separation persisted can be inferred by considering the accretion times of the youngest meteorite parent bodies in each reservoir. This is because in the ε^{95}Mo–ε^{94}Mo diagram (Fig. 1), no meteorites plot between the CC and NC lines, meaning that the NC and CC reservoirs cannot have mixed but instead must have remained isolated from each other until parent body accretion in the NC and CC reservoirs terminated. As accretion of chondrite parent bodies occurred at ∼2 My after CAI formation in the NC reservoir (ordinary chondrites) and until ∼3–4 My in the CC reservoir (CC chondrites) (18–20), this means that the NC and CC reservoirs must have remained isolated from each other from <1 My until at least ∼3–4 My after CAI formation. This prolonged spatial separation of the NC and CC reservoirs cannot simply reflect a large distance between these reservoirs within the disk, because the rapid speed of grain drift in the disk would have facilitated efficient mixing on much shorter timescales (21, 22). One way to avoid the inward drift of material would be the rapid accumulation of these grains into planetesimals. However, this also cannot explain the efficient separation of the NC and CC reservoirs, because in both reservoirs planetesimal accretion occurred concurrently for several million years. Consequently, the precursor dust of planetesimals in both reservoirs must have been present for this period and, therefore, cannot have been locked up in earlier-formed planetesimals.

The most plausible mechanism to efficiently separate two disk reservoirs for an extended period is the accretion of a giant planet in between them, generating a gap within the disk and inhibiting the inward drift of dust grains (13, 23, 24) (Fig. 4). Being the largest and nearest gas-giant planet, Jupiter is the most likely candidate for separating the NC and CC reservoirs. As the Earth is part of the NC reservoir, this implies that the CC reservoir was initially located outside Jupiter's orbit, meaning that CC bodies originally derive from the outer Solar System. Because the CC meteorites include some iron meteorites, one important implication of our data is that early and rapid formation of differentiated planetesimals was possible not only in the innermost terrestrial planet region (25), but also farther out in the disk.

The formation of Jupiter between the NC and CC reservoirs not only provides a mechanism for efficiently separating these two reservoirs for an extended period, but also provides a means for the later transport of CC bodies into the inner Solar System. This is necessary because although the NC and CC bodies initially formed in spatially distinct areas of the disk, at the present day they both reside in the main asteroid belt. This is a natural outcome of the growth of Jupiter, which ultimately leads to scattering of bodies from beyond Jupiter's orbit (i.e., CC bodies) into the inner Solar System, either during an inward-then-outward migration of Jupiter (10, 23) or during runaway growth of Jupiter on a fixed orbit (26). Thus, the presence of Jupiter between the NC and CC reservoirs provides the most plausible mechanism to

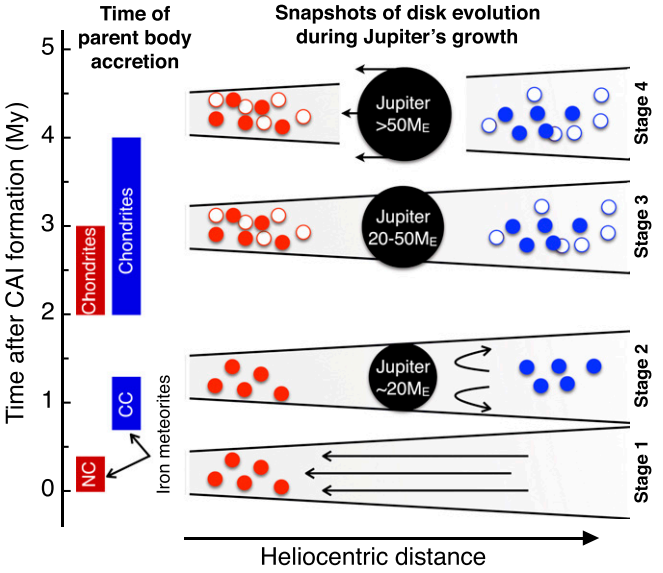

Fig. 4. Four snapshots of Jupiter's growth in the solar circumstellar disk. At stage 1, within <0.4 My after CAI, the NC iron meteorite parent bodies (red solid symbols) accreted in a continuous gas disk characterized by inward drag of solids. At stage 2, around ∼1 My after CAI, iron meteorite parent bodies of the CC reservoir (blue solid symbols) had accreted and Jupiter had already grown to ∼20 M_E, preventing any inward drag of solids (24). At stage 3, from ∼2 My to ∼4 My after CAI, Jupiter grew further through gas accretion onto its core. Moreover, the ordinary chondrite parent bodies (red open symbols) accreted in the NC reservoir and CC chondrite parent bodies (blue open symbols) in the CC reservoir. At stage 4, after ∼3–4 My after CAI, Jupiter had grown to ∼50 M_E and had opened a gap in the disk (13, 23, 24), likely resulting in the inward migration of Jupiter. Solid boxes (*Left*) show the accretion ages of iron meteorite and chondrite parent bodies in the NC and CC reservoirs (see *CC and NC Iron Meteorites*).

account for both (*i*) the prolonged spatial separation of these reservoirs and (*ii*) the co-occurrence of NC and CC bodies in the present-day asteroid belt.

Growth History of Jupiter

With the assumption that the prolonged spatial separation of the NC and CC reservoirs reflects the formation of Jupiter in between these reservoirs, the distinct timescales for the accretion of NC and CC meteorite parent bodies make it possible to date the formation of Jupiter. The growth of Jupiter beyond a certain mass would have inhibited the inward drift of particles (13, 24), and once it grew further, Jupiter ultimately would have generated a gap within the disk (23). In particular, theoretical studies suggest that the inward drift of particles stopped once Jupiter's core had grown to about 20 M_E (24), while a gap formed once Jupiter reached approximately 50 M_E (13, 23, 27). Thus, because the *r*-process material that was added to the CC reservoir did not infiltrate the coexisting yet spatially separated NC reservoir, this implies that at the time the *r*-process material was added, Jupiter already had a size of >20 M_E. Furthermore, because this material must have been added and homogenized before the first planetesimals formed within the CC reservoir at ∼1 My after CAI formation, these results mandate that Jupiter reached a size of >20 M_E within ∼1 My of Solar System formation (Fig. 4). This early formation of (proto-) Jupiter is consistent with the rapid growth of Jupiter's core predicted in theoretical models (1, 4), regardless of whether pebble accretion (28, 29) or hierarchical growth models (30, 31) are assumed.

Once Jupiter reached a mass of 50 M_E, which happens via gas accretion onto its solid core, a gap opened in the disk (13, 23, 24, 27), followed by scattering of bodies from beyond Jupiter's orbit (i.e., CC bodies) into the inner Solar System (10, 23, 26). Our results show that this scattering of CC bodies and, hence, Jupiter's outward migration or runaway growth cannot have started before ∼3–4 My after CAI formation. This is because CC chondrite parent bodies continued to form until at least ∼3–4 My after CAI formation (18–20). As these chondrites plot on the CC line in Mo isotope space (Fig. 1), they must have formed before the scattering of CC meteorites into the inner Solar System and, hence, before the CC meteorite parent bodies joined the NC parent bodies in the asteroid belt. Accordingly, these data indicate that Jupiter reached ∼50 M_E later than ∼3–4 My after CAI formation. This is consistent with theoretical predictions that the rapid growth of Jupiter's core to ∼20 M_E was followed by a more protracted stage of gas and solid accretion to several tens of Earth's masses (1, 32, 33) before runaway gas accretion led to Jupiter's final mass (∼318 M_E). Thus, our results are in good agreement with the timing and sequence of events predicted in the core accretion model for the formation of Jupiter (1). One important implication of this result is that, because Jupiter acted as a barrier against inward transport of solids across the disk, the inner Solar System remained relatively mass deficient, possibly explaining its lack of any "super-Earths" (34, 35).

Materials and Methods

For this study we selected a total of 19 samples covering six different rare iron meteorite groups (IC, IIC, IID, IIF, IIIE, and IIIF). This sample set complements the iron meteorites from major groups (IIAB, IID, IIIAB, IVA, and IVB) whose W, Pt, and Mo isotope compositions had previously been analyzed (6, 15). After digestion of the iron meteorites in concentrated HNO_3–HCl (2:1), the sample solutions were split into a fraction for W and Mo (∼90%) and for Pt (∼10%) isotope analysis. The chemical separation of W, Pt, and Mo was accomplished using ion exchange chromatography following previously published procedures (6, 12, 15, 36). The W, Pt, and Mo isotope compositions were measured on a ThermoScientific Neptune *Plus* MC-ICPMS in the Institut für Planetologie at the University of Münster (12, 15, 36) (see *SI Materials and Methods* for details). Instrumental mass bias was corrected by internally normalizing to $^{186}W/^{184}W = 0.92767$, $^{198}Pt/^{195}Pt = 0.2145$, and $^{98}Mo/^{96}Mo = 1.453173$, using the exponential law. The W, Pt, and Mo isotope data are reported as ε-unit (i.e., parts per 10^4) deviation relative to the isotopic ratios measured for terrestrial bracketing solution standards. The reported ε^iW, ε^iPt, and ε^iMo values for samples (Tables S1–S4) represent the mean of pooled solution replicates (n = 1–8) together with their associated uncertainties [2 SD or 95% confidence (conf.) interval].

ACKNOWLEDGMENTS. We gratefully acknowledge the Natural History Museum, London (C. Smith, N. Almeida) and the Field Museum, Chicago (P. Heck) for providing samples. We thank F. Nimmo for giving detailed insights into giant planet formation and for a first draft of Fig. 4. We also thank G. Brennecka and A. Morbidelli for discussions; C. Brennecka for comments on the paper; and S. Gerber, J. Hellmann, N. Krabbe, and U. Heitmann for their assistance. Finally, we thank Alex Halliday and two anonymous reviewers for their constructive comments that helped to improve the paper. This study was performed under the auspices of the US DOE by Lawrence Livermore National Laboratory under Contract DE-AC52-07NA27344 with release number LLNL-JRNL-731226. This work was funded by the Deutsche Forschungsgemeinschaft (DFG) (Collaborative Research Center/Transregio TRR 170 subproject B3-1). C.B. was supported by the European Research Council Consolidator grant ISOCORE (Contract 616564), and G.B. was supported by the DFG Priority Program 1385 (Grant KL1857/3). This is TRR 170 publication 10.

1. Pollack JB, et al. (1996) Formation of the giant planets by concurrent accretion of solids and gas. *Icarus* 124:62–85.
2. Mizuno H, Nakazawa K, Hayashi C (1978) Instability of a gaseous envelope surrounding a planetary core and formation of giant planets. *Prog Theor Phys* 60:699–710.
3. Haisch KE, Lada EA, Lada CJ (2001) Disk frequencies and lifetimes in young clusters. *Astrophys J* 553:L153–L156.
4. Helled R, et al. (2014) *Giant Planet Formation, Evolution, and Internal Structure. Protostars and Planets VI* (Univ of Arizona Press, Tucson, AZ).
5. Dauphas N, Schauble EA (2016) Mass fractionation laws, mass-independent effects, and isotopic anomalies. *Annu Rev Earth Planet Sci* 44:709–783.
6. Burkhardt C, et al. (2011) Molybdenum isotope anomalies in meteorites: Constraints on solar nebula evolution and origin of the Earth. *Earth Planet Sci Lett* 312:390–400.
7. Trinquier A, Birck J, Allegre CJ (2007) Widespread ^{54}Cr heterogeneity in the inner solar system. *Astrophys J* 655:1179–1185.
8. Trinquier A, et al. (2009) Origin of nucleosynthetic isotope heterogeneity in the solar protoplanetary disk. *Science* 324:374–376.
9. Levison HF, et al. (2009) Contamination of the asteroid belt by primordial trans-Neptunian objects. *Nature* 460:364–366.
10. Walsh KJ, Morbidelli A, Raymond SN, O'Brien DP, Mandell AM (2011) A low mass for Mars from Jupiter's early gas-driven migration. *Nature* 475:206–209.
11. Warren P (2011) Stable-isotopic anomalies and the accretionary assemblage of the Earth and Mars: A subordinate role for carbonaceous chondrites. *Earth Planet Sci Lett* 311:93–100.
12. Budde G, et al. (2016) Molybdenum isotopic evidence for the origin of chondrules and a distinct genetic heritage of carbonaceous and non-carbonaceous meteorites. *Earth Planet Sci Lett* 454:293–303.
13. Morbidelli A, et al. (2016) Fossilized condensation lines in the Solar System protoplanetary disk. *Icarus* 267:368–376.
14. Van Kooten EMME, et al. (2016) Isotopic evidence for primordial molecular cloud material in metal-rich carbonaceous chondrites. *Proc Natl Acad Sci USA* 113:2011–2016.
15. Kruijer TS, et al. (2014) Protracted core formation and rapid accretion of protoplanets. *Science* 344:1150–1154.
16. Qin L, Dauphas N, Wadhwa M, Masarik J, Janney PE (2008) Rapid accretion and differentiation of iron meteorite parent bodies inferred from ^{182}Hf–^{182}W chronometry and thermal modeling. *Earth Planet Sci Lett* 273:94–104.
17. Kleine T, Mezger K, Palme H, Scherer E, Münker C (2005) Early core formation in asteroids and late accretion of chondrite parent bodies: Evidence from ^{182}Hf–^{182}W in CAIs, metal-rich chondrites, and iron meteorites. *Geochim Cosmochim Acta* 69:5805–5818.
18. Kita NT, Ushikubo T (2012) Evolution of protoplanetary disk inferred from ^{26}Al chronology of individual chondrules. *Meteorit Planet Sci* 47:1108–1119.
19. Connelly JN, et al. (2012) The absolute chronology and thermal processing of solids in the solar protoplanetary disk. *Science* 338:651–655.
20. Schrader DL, et al. (2016) Distribution of ^{26}Al in the CR chondrite chondrule-forming region of the protoplanetary disk. *Geochim Cosmochim Acta* 201:275–302.
21. Weidenschilling SJ (1977) Aerodynamics of solid bodies in the solar nebula. *Mon Not R Astron Soc vol* 180:57–70.
22. Birnstiel T, Dullemond CP, Pinilla P (2013) Lopsided dust rings in transition disks. *Astron Astrophys* 550:L8.
23. Lin DNC, Papaloizou J (1986) On the tidal interaction between protoplanets and the protoplanetary disk. III - Orbital migration of protoplanets. *Astrophys J* 309:846.
24. Lambrechts M, Johansen A, Morbidelli A (2014) Separating gas-giant and ice-giant planets by halting pebble accretion. *Astron Astrophys* 572:A35.
25. Bottke WF, Nesvorný D, Grimm RE, Morbidelli A, O'Brien DP (2006) Iron meteorites as remnants of planetesimals formed in the terrestrial planet region. *Nature* 439:821–824.
26. Kretke KA, Levison HF, Bottke W (2016) Exploring how giant planet formation affected the asteroid belt. *Proceedings of the 48th Meeting of the Division for Planetary Sciences* (Am Astron Soc, Washington, DC), abstract 25.

27. Crida A, Morbidelli A, Masset F (2006) On the width and shape of gaps in protoplanetary disks. *Icarus* 181:587–604.
28. Lambrechts M, Johansen A (2012) Rapid growth of gas-giant cores by pebble accretion. *Astron Astrophys* 544:A32.
29. Levison HF, Kretke KA, Duncan MJ (2015) Growing the gas-giant planets by the gradual accumulation of pebbles. *Nature* 524:322–324.
30. Kokubo E, et al. (2002) Formation of protoplanet systems and diversity of planetary systems. *Astrophys J* 581:666–680.
31. Desch SJ, et al. (2007) Mass distribution and planet formation in the solar nebula. *Astrophys J* 671:878–893.
32. Monga N, Desch S (2014) External photoevaporation of the solar nebula: Jupiter's noble gas enrichments. *Astrophys J* 798:9.
33. Johnson BC, Walsh KJ, Minton DA, Krot AN, Levison HF (2016) Timing of the formation and migration of giant planets as constrained by CB chondrites. *Sci Adv* 2: e1601658.
34. Izidoro A, Raymond SN, Morbidelli A, Hersant F, Pierens A (2015) Gas giant planets as dynamical barriers to inward-migrating super-Earths. *Astrophys J* 800:L22.
35. Morbidelli A, Raymond SN (2016) Challenges in planet formation. *J Geophys Res* 121: 1962–1980.
36. Kruijer TS, et al. (2013) Neutron capture on Pt isotopes in iron meteorites and the Hf–W chronology of core formation in planetesimals. *Earth Planet Sci Lett* 361:162–172.
37. Nicolussi GK, et al. (1998) Molybdenum isotopic composition of individual presolar silicon carbide grains from the Murchison meteorite. *Geochim Cosmochim Acta* 62: 1093–1104.
38. Prombo CA, Clayton RN (1993) Nitrogen isotopic compositions of iron meteorites. *Geochim Cosmochim Acta* 57:3749–3761.
39. Marty B, Chaussidon M, Wiens RC, Jurewicz AJ, Burnett DS (2011) A ^{15}N-poor isotopic composition for the solar system as shown by Genesis solar wind samples. *Science* 332: 1533–1536.
40. Rehkämper M, Halliday ANN (1997) Development and application of new ion-exchange techniques for the separation of the platinum group and other siderophile elements from geological samples. *Talanta* 44:663–672.
41. Kruijer TS, et al. (2012) Hf–W chronometry of core formation in planetesimals inferred from weakly irradiated iron meteorites. *Geochim Cosmochim Acta* 99:287–304.
42. Willbold M, Elliott T, Moorbath S (2011) The tungsten isotopic composition of the Earth's mantle before the terminal bombardment. *Nature* 477:195–198.
43. Budde G, Kruijer TS, Fischer-Gödde M, Kleine T (2015) Planetesimal differentiation revealed by the Hf-W systematics of ureilites. *Earth Planet Sci Lett* 430:316–325.
44. Kruijer TS, Kleine T, Fischer-Gödde M, Burkhardt C, Wieler R (2014) Nucleosynthetic W isotope anomalies and the Hf-W chronometry of Ca-Al-rich inclusions. *Earth Planet Sci Lett* 403:317–327.
45. Kruijer TS, Kleine T, Fischer-Gödde M, Sprung P (2015) Lunar tungsten isotopic evidence for the late veneer. *Nature* 520:534–537.
46. Cook DL, Kruijer TS, Leya I, Kleine T (2014) Cosmogenic ^{180}W variations in meteorites and re-assessment of a possible ^{184}Os–^{180}W decay system. *Geochim Cosmochim Acta* 140:160–176.
47. Cook DL, Schönbächler M (2016) High-precision measurement of W isotopes in Fe–Ni alloy and the effects from the nuclear field shift. *J Anal At Spectrom* 31:1400–1405.
48. Masarik J (1997) Contribution of neutron-capture reactions to observed tungsten isotopic ratios. *Earth Planet Sci Lett* 152:181–185.
49. Leya I, Wieler R, Halliday AN (2003) The influence of cosmic-ray production on extinct nuclide systems. *Geochim Cosmochim Acta* 67:529–541.
50. Budde G, Kleine T, Kruijer TS, Burkhardt C, Metzler K (2016) Tungsten isotopic constraints on the age and origin of chondrules. *Proc Natl Acad Sci USA* 113:2886–2891.
51. Burkhardt C, Kleine T, Dauphas N, Wieler R (2012) Nucleosynthetic tungsten isotope anomalies in acid leachates of the Murchison chondrite: Implications for hafnium-tungsten chronometry. *Astrophys J* 753:L6.
52. Qin L, et al. (2008) Tungsten nuclear anomalies in planetesimal cores. *Astrophys J* 674: 1234–1241.
53. Wittig N, Humayun M, Brandon D, Huang S, Leya I (2013) Coupled W–Os–Pt isotope systematics in IVB iron meteorites: In situ neutron dosimetry for W isotope chronology. *Earth Planet Sci Lett* 361:152–161.
54. Burkhardt C, Schönbächler M (2015) Intrinsic W nucleosynthetic isotope variations in carbonaceous chondrites: Implications for W nucleosynthesis and nebular vs. parent body processing of presolar materials. *Geochim Cosmochim Acta* 165:361–375.
55. Walker RJ (2012) Evidence for homogeneous distribution of osmium in the protosolar nebula. *Earth Planet Sci Lett* 351–352:36–44.
56. Qin L, Dauphas N, Horan MF, Leya I, Carlson RW (2015) Correlated cosmogenic W and Os isotopic variations in Carbo and implications for Hf–W chronology. *Geochim Cosmochim Acta* 153:91–104.
57. Kleine T, et al. (2009) Hf–W chronology of the accretion and early evolution of asteroids and terrestrial planets. *Geochim Cosmochim Acta* 73:5150–5188.
58. Vockenhuber C, et al. (2004) New half-life measurement of 182Hf: Improved chronometer for the early solar system. *Phys Rev Lett* 93:172501.
59. Neumann W, Breuer D, Spohn T (2012) Differentiation and core formation in accreting planetesimals. *Astron Astrophys* 543:A141.
60. Hevey PJ, Sanders IS (2006) A model for planetesimal meltdown by 26Al and its implications for meteorite parent bodies. *Meteorit Planet Sci* 41:95–106.
61. Norris TL, Gancarz AJ, Roico DJ, Thomas KW (1983) Half-life of 26Al. Proc 14th Lunar Planet Sci Conf 88:331–333.
62. Lodders K, Fegley B (1998) *The Planetary Scientist's Companion* (Oxford Univ Press, New York).
63. Taylor GJ (1992) Core formation in asteroids. *J Geophys Res* 97:14717.
64. McCoy TJ, Mittlefehldt DW, Wilson L (2006) Asteroid differentiation. *Meteorites and the Early Solar System II*, eds Lauretta DS, McSween HYJ (Univ of Arizona Press, Tucson, AZ), pp 733–745.